GaN AND RELATED MATERIALS FOR HIGH POWER APPLICATIONS

M.S. SHUR

Electrical, Computer, and Systems Engineering and Center for Integrated Electronics and Electronics Manufacturing
Rensselaer Polytechnic Institute, Troy, NY 12180-3590
shurm@rpi.edu

ABSTRACT

Unique properties of GaN and related semiconductors make them superior for high-power applications. The maximum density of the two-dimensional electron gas at the GaN/AlGaN heterointerface or in GaN/AlGaN quantum well structures can reach $5x10^{13}$ cm^{-2}, which is more than an order of magnitude higher than for traditional GaAs/AlGaAs heterostructures. The mobility-sheet carrier concentration product for these two dimensional systems might also exceed that for GaAs/AlGaAs heterostructures and can be further enhanced by doping the conducting channels and by using "piezoelectric" doping, which takes advantage of high piezoelectric constants of GaN and related materials. We estimate that current densities over 20 A/mm can be reached in GaN-based High Electron Mobility Transistors (HEMTs). These high current values can be combined with very high breakdown voltages in high-power HEMTs. These breakdown voltages are expected to reach several thousand volts. Recent Monte Carlo simulations point to strong ballistic and overshoot effects in GaN and related materials, which should be even more pronounced than in GaAs-based compounds but at much higher electric fields. This should allow us to achieve faster switching, minimizing the power dissipation during switching events. Self-heating, which is unavoidable in power devices, raises operating temperatures of power devices well above the ambient temperature. For GaN-based devices, the use of SiC substrates having high thermal conductivity is essential for ensuring an effective heat dissipation. Such an approach combines the best features of both GaN and SiC technologies; and GaN/SiC-based semiconductors and heterostructures should find numerous applications in power electronics.

1. INTRODUCTION

An ideal semiconductor material for power applications should possess excellent transport and thermal properties, a high breakdown voltage, chemical inertness, mechanical stability and should allow us to fabricate both unipolar and bipolar devices with low parasitics. Traditionally, most of the power devices today are made from silicon or GaAs. However, wide band gap semiconductor materials have attracted a lot of attention as potential candidates for high power applications.

SiC devices have been evaluated for high-power, high-voltage applications. Their operation is projected for voltages exceeding 1 kV. [1] More recently, GaN-based devices grown on sapphire substrates also demonstrated high current-carrying capabilities and high breakdown voltages (see, for example, [2]). The potential of GaN-based devices for high power has been boosted by the demonstration of GaN/AlGaN Heterostructure Field Effect Transistors (DC-HEMTs) on SiC substrates [3-4] and by the recent demonstration of Double Channel GaN/AlGaN HEMTs. [5]

In Section 2, we discuss transport properties of GaN and related heterostructures, which make them superior for high-power, high temperature applications. These properties affect the design of power devices and, in many cases, suggest design solutions different from those for more conventional semiconductor materials. In Section 3, we analyze the properties of the two-dimensional electron gas at the GaN/AlGaN heterointerfaces and in the quantum well structures and superlattices. In Section 4, we discuss the significance of the piezoelectric effect for GaN/AlGaN heterostructures. In Section 5, we consider the current-carrying capabilities and breakdown voltages of GaN-based HEMTs. Section 6 gives a brief review of recent results on self-heating in GaN-based HEMTs and on GaN-based HEMTs grown on SiC substrates.

Mat. Res. Soc. Symp. Proc. Vol. 483 © 1998 Materials Research Society

2. TRANSPORT PROPERTIES of GaN.

Fig. 1 compares the calculated temperature dependencies of the electron mobility in bulk GaN and GaAs with and without accounting for the impurity scattering. The calculations were done using the theory developed by Shur et al. (1996). As can be seen, the electron mobility in bulk GaN is less sensitive to ionized impurity scattering than that in GaAs.

Since the atomic radius of Al is the same as that of Ga (1.26 Å), many semiconductors that contain different molar fractions of Al and Ga but the same anion sublattice form excellent heterostructures. The AlGaAs/ GaAs heterostructure is a classic example. Other examples include AlInAs and GaInAs. The AlGaN/GaN heterostructure is not an exception, and close values of the lattice constants for AlN and GaN lead to a good quality heterointerface. The first evidence of the existence of the two-dimensional electron gas at the GaN/AlGaN heterointerface was provided by a large mobility enhancement at the heterointerface. Khan et al. [6] observed a large mobility enhancement in the two dimensional (2D) electron gas at the AlGaN/GaN interface. They measured the 2D electron gas Hall mobility around 5,000 $cm^2/V\text{-}s$ at 80 K, compared to the maximum electron mobility of approximately 1,200 $cm^2/V\text{-}s$ in their bulk doped GaN samples. The room temperature Hall mobilities were 800 $cm^2/V\text{-}s$ and 500 $cm^2/V\text{-}s$ for the 2D electron gas and electrons in bulk GaN, respectively. The value of the sheet concentration determined from the Hall data was on the order of 2.5×10^{11} cm^{-2}, smaller than that value in many AlGaAs/GaAs modulation doped structures. More recently, Gaska et al. [7] reported on the electron mobility in the 2D-gas electron gas at the GaN/AlGaN interface exceeding 10,000 $cm^2/V\text{-}s$ at cryogenic temperatures and exceeding 2000 $cm^2/V\text{-}s$ at room temperature. These values were observed in the samples with very high sheet carrier concentration (on the order of 10^{13} cm^{-2}).

In the two dimensional electron gas at the GaN/AlGaN interface, the electron mobility in comparably doped GaN is higher because a high sheet electron density, n_s, at the heterointerface screens the ionized impurities and diminishes scattering. This is illustrated in Fig. 2, which shows the electron mobility in GaN at 300 K as a function of the electron concentration for different concentrations of ionized impurities. (In this calculation, we used the bulk scattering rates with screening and assumed the effective bulk scattering rate.)

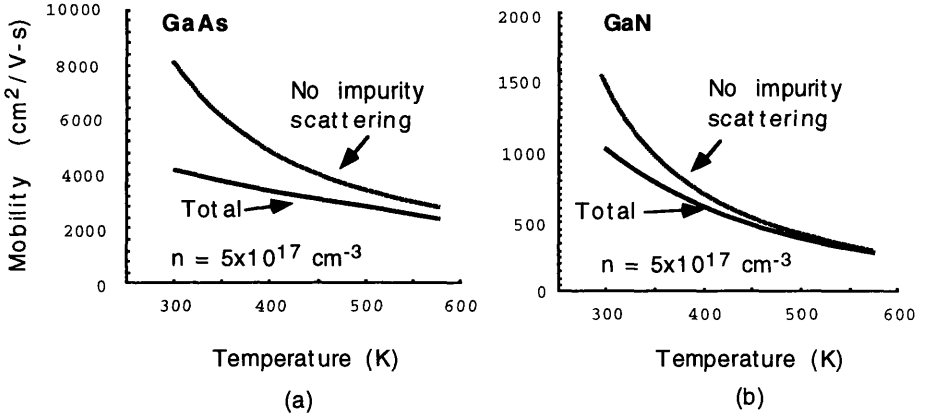

Figure 1: Calculated temperature dependencies of the electron mobility in GaAs (a) and GaN (b) with and without accounting for the impurity scattering.

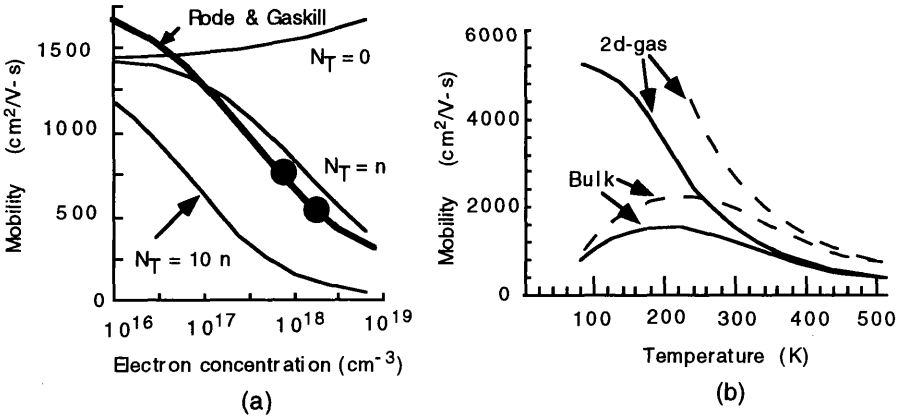

Figure 2: Electron Hall mobility in bulk GaN versus electron carrier concentration for different compensation levels at 300 K (a) and electron Hall mobility in GaN versus temperature for two dimensional electron gas and bulk GaN (b). Thick solid line and dots in Fig. 2 a show the dependence calculated by Rode and Gaskill [8] and experimental data for cubic GaN by Kim et al. [9], respectively. In Fig. 2b, for the bulk calculation, $n = 2x10^{16}$ cm^{-3}, $N_T = 2x10^{17}$ cm^{-3}; for the 2DEG calculation, $n = 5x10^{17}$ cm^{-3}, $N_T = 6.5x10^{16}$ cm^{-3}. Dashed lines in Fig. 2 b corresponsd to 3C-GaN. (After [10].)

The results shown in Figures 1 and 2 suggest the introduction of dopants in GaN does not change the electron mobility too much.

Fig. 3 shows the computed velocity-field characteristics of GaN and GaAs at different temperatures.

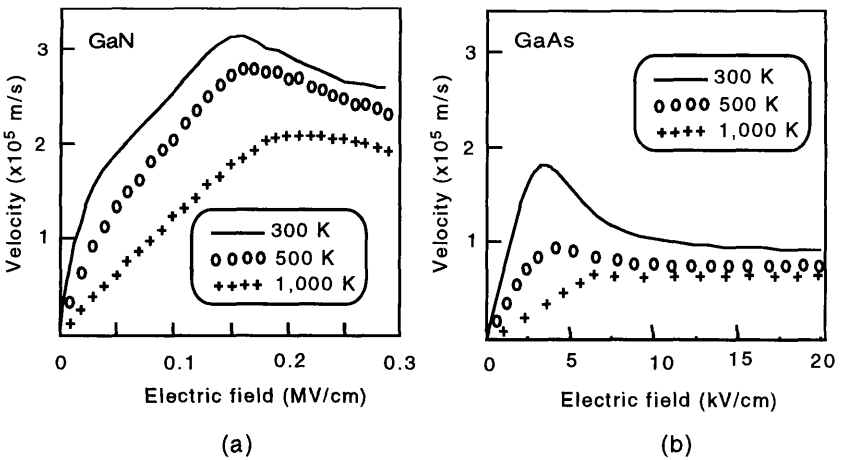

Figure 3: Velocity-field characteristics of GaN (a) and GaAs (b) at different temperatures. Fig. 3a is after [11]. Fig. 3b is computed using the fit to the Monte Carlo calculations reported in [12] for the following values of the low field mobility: 7,000 $cm^2/V\text{-}s$ at 300 K, 3,000 $cm^2/V\text{-}s$ at 500 K, and 1,100 $cm^2/V\text{-}s$ at 1,000 K.

As can be seen from that figure, the electron velocity in GaN is less sensitive to temperature than that of GaAs. Hence, GaN devices should be more tolerant to self-heating and clearly more suitable for high temperature operation.

Fig. 4 shows the computed velocity of electrons injected with low velocities into a constant electric field region into GaN and GaAs. As can be seen from the figure, GaN exhibit much more pronounced overshoot effects even compared to GaAs but at much higher electric fields. This result illustrates the potential of GaN for ballistic power devices.

Figures 3 and 4 clearly demonstrate the superiority of the GaN transport properties for high-temperature, high-power applications.

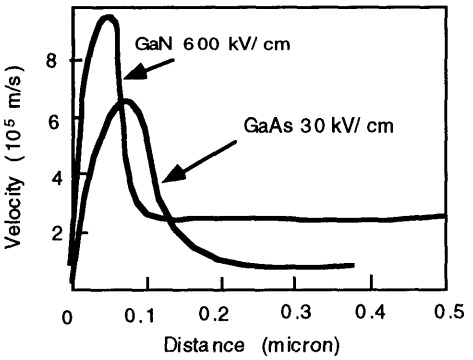

Figure 4: Computed velocity of electrons injected with low velocities into a constant electric field region into GaN and GaAs (after [13]).

A very intriguing possibility is to use InN for a device channel. This material is expected to have a much higher mobility (3,200 cm^2/V-s) at room temperature, a much higher peak velocity, and much more pronounced overshoot and ballistic effects (see [14] and [15] for more details).

3. TWO DIMENSIONAL ELECTRON GAS AT GaN/AlGaN INTERFACE

Cyclotron Resonance and Quantum Hall Effect studies of electrons confined at the GaN-AlGaN interface prove the existence of the two-dimensional electron gas at this heterointerface. [16]

According to Stern and Sarma [17], the 2D electron gas density is given by

$$n_S = Dk_BT \sum_{j=1}^{l} \ln\left[1+\exp\left(\frac{E_F - E_j}{k_BT}\right)\right]. \qquad (1)$$

Here l is the total number of subbands, k_B is the Boltzmann constant, T is temperature, E_F is the Fermi level, E_j are the subband energy levels, $D = \frac{m_n}{\pi\hbar^2}$ is the density of states for one subband, m_n is the effective mass. The subband energy levels are given by

$$E_j - E_c(0) = \left(\frac{9\pi^2\hbar^2q^2F_{eff}^2}{8m_n}\right)^{1/3}\left(j+\frac{3}{4}\right)^{2/3}, \qquad (2)$$

where $E_c(0)$ is the minimum conduction band energy at the heterointerface. For an n^+-n type heterostructure, the effective field, $F_{eff} = F_s/2$ where the surface field, $F_s = q\ n_s/\varepsilon_s$, q is the electronic charge, ε_S is the GaN dielectric permittivity, and n_s is the interface electron sheet density. Fig. 5 shows the dependence of E_F on n_s (counted from the bottom of the conduction band in GaN at the heterointerface) calculated using Eqs. (1) and (2). Also shown is the Al molar fraction, which corresponds to the value of the conduction band discontinuity equal to the position of the Fermi level counted from the bottom of the conduction band at the heterointerface. The effective mass of 0.24 m_e (where m_e is the free electron mass) was assumed in this calculation. The first seven subbands were accounted for. For n_s higher than $1.5\text{x}10^{12}$ cm^{-2}, the following approximation:

$$E_F = E_o + n_s/D, \tag{3}$$

is in excellent agreement with the computed dependence.

As can be seen, values of n_s close to $2\text{x}10^{13}$ cm^{-2} can be achieved for relatively low Al molar fractions. These values correspond to the surface field of nearly 4 MV/cm! Such high concentrations are not achievable in AlGaAs/GaAs heterostructures, and such an interface field may be too high for relatively narrow gap materials leading to breakdown. Even more exotic heterostructures, such as AlInAs/InGaAs, with a larger conduction band discontinuity than AlGaAs/GaAs, cannot achieve such high values of n_s. However AlGaN should be able to withstand the high fields required for the modulation of such high electron sheet concentrations.

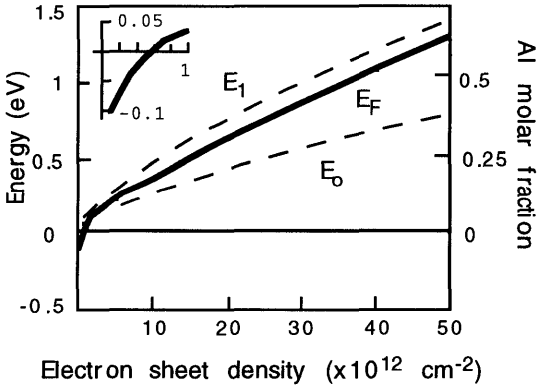

Figure 5: Fermi level (solid line) and the positions of the ground and first excited subbands for GaN/AlGaN heterostructure counted from the bottom of the conduction band in GaN at the heterointerface. The insert shows the position of the Fermi level at small values of n_s. Also shown the Al molar fraction, with corresponds to the value the conduction band discontinuity equal to the energy scale on the left.

Even higher values of n_s in the AlGaN/GaN heterostructures can be achieved by doping the active layer so the total surface electron concentration in the channel

$$N_S = n_S + N_d d. \tag{4}$$

Even more important is the change in the band diagram caused by the channel doping. This is illustrated by Fig. 6, which compares the band diagrams of the GaN heterostructures close to heterointerface for doped and undoped GaN layers. As can be seen, in the doped quantum well

structures, electrons can go into bulk states, whose density is enough to contain a very large electron sheet density.

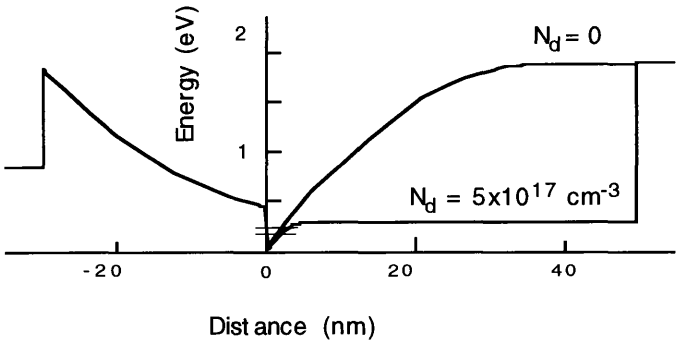

Figure 6: Band diagrams of the GaN heterostructures for doped and undoped GaN layers. The short horizontal lines show the position of the Fermi level (top line) and of the lowest subband (bottom line). Notice the difference in the electric field slopes in GaN and AlGaN related to piezoeffect (see Section 4). The Al mole fraction is x=0.2, the Schottky barrier height is 1 eV, the conduction band discontinuity, $\Delta E_c = 0.75\ \Delta E_g$, AlGaN doping is $5x10^{18}$ cm^{-3}, the 2D gas density is $5x10^{12}$ cm^{-2}. T=300 K. Other parameters used in the calculation are given in Table 1.

Table 1. GaN and AlN parameters.

Parameter *	**AlN**	**GaN**
static dielectric constant	8.5	8.9
energy gap (eV)	6.2	3.4
piezoelectric constant e_{31} (C/m^2)	-0.58	-0.36
piezoelectric constant e_{33} (C/m^2)	1.55	1
elastic module c_{31} (Gpa)	158	99
elastic module c_{33} (Gpa)	267	389
lattice constant, a (Å)	3.112	3.189
electron effective mass (m_e)	-	0.23
hole effective mass (m_h)	-	1

* Material parameters of AlGaN were determined by taking a linear interpolation between GaN and AlN parameters as functions of the Al molar fraction.

Based on Fig. 5, we estimate that the values of n_s as high as $5x10^{13}$ cm^{-2} can be obtained in doped channel AlGaN/GaN heterostructures leading to superior current-carrying capabilities of these devices.

4. ROLE OF PIEZOELECTRIC EFFECT

GaN and, especially AlN, have strongly pronounced piezoelectric properties. The crystal growth direction for these heterostructures (in the c-axis direction) is such that these properties directly affect the electric field in the direction perpendicular to the heterointerface.

Bykhovski et al. [18-23], Yu et al. [24], and Gaska et al. [25-27] reported on the results of the studies of strain, piezoelectric effects, and piezoresistive effects in GaN/AlGaN heterostructures. Gaska et al. [25] calculated $Al_xGa_{1-x}N/GaN$ band structure by solving the Poisson equation numerically and using the Fermi-Dirac distribution function for the electrons. Just as in our calculations in Section 3, they assumed the conduction band discontinuity to be equal to 75% of the band gap discontinuity (as suggested by Martin et al. [28]). The boundary condition for the $Al_xGa_{1-x}N/GaN$ interface accounts for the piezoeffect:

$$\varepsilon_1 F_1 + P_1 = \varepsilon_2 F_2, \tag{5}$$

where ε_1 and ε_2 are the dielectric constants, and F_1, F_2 are the interface values of the electric field in $Al_xGa_{1-x}N$ and GaN, correspondingly, and P_1 is the piezoelectric polarization in $Al_xGa_{1-x}N$. [18] For the (0001) growth direction, it can be expressed in terms of the $Al_xGa_{1-x}N$ piezoelectric coefficients e_{31}, e_{33} as follows:

$$P_1 = \pm 2(e_{31} - e_{33}c_{31} / c_{33})u_{xx}. \tag{6}$$

Here c_{31}, c_{33} are the $Al_xGa_{1-x}N$ elastic constants and u_{xx} is the strain component in the interface plane. If the strain is not relaxed by the dislocations, then the strain component is given by

$$u_{xx} = a_{GaN}/a_{AlGaN} - 1. \tag{7}$$

Preliminary experimental results seem to indicate that the Al molar fraction may be graded at the heterointerface over distances of the order of 20 Å. [25] This should increase the critical thickness for the elastic strain relaxation compared to the critical thickness for ideally abrupt heterostructures. Hence, the piezoeffect may be important in AlGaN/GaN HEMTs with $Al_{0.2}Ga_{0.8}N/GaN$ thickness of 300 Å, which is larger than the critical thickness (160 Å). [18]

Gaska et al. [23] estimated e_{31}, e_{33} of $Al_xGa_{1-x}N$ using the linear interpolation between corresponding GaN and AlN piezoelectric constants, which are given by Bykhovski et al. [29] The negative sign in Eq. (6) corresponds to a top nitrogen plane, with coefficients e_{31}, e_{33} being defined by Bykhovski et al. [29]. Fig. 7 shows the calculated band diagrams for the AlGaN/GaN HFET with a 300 Å thick $Al_{0.2}Ga_{0.8}N/GaN$ barrier layer doped with 10^{18} cm^{-3} donors.

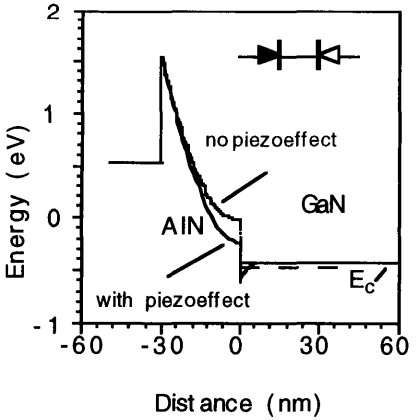

Figure 7: Calculated band diagrams of the $Al_{0.2}Ga_{0.8}N/GaN$ HEMTs accounting for the piezoeffect and neglecting the piezoeffect at gate voltage of -1V. [23] Donor concentration in $Al_{0.2}Ga_{0.8}N/GaN$ is 10^{18} cm^{-3}. Also shown is the two-diode equivalent circuit. The diode controlling the gate current is shown in black. The doping density in the GaN layer is $5x10^{17}$ cm^{-3}. Other parameters are given in Table 1.

Even a more dramatic change in the band diagrams is related to the two different top atomic plane configurations (corresponding to two different signs in eq. (6). This is illustrated by Fig. 8 that shows the band diagram for the same parameters as for Fig. 6 but for the opposite top atomic plane configuration. As can be seen from this figure, the same sheet carrier concentration in GaN is achieved at a much higher positive bias. This corresponds to a large positive shift in the threshold voltage (on the order of 7 V for this particular set of parameters).

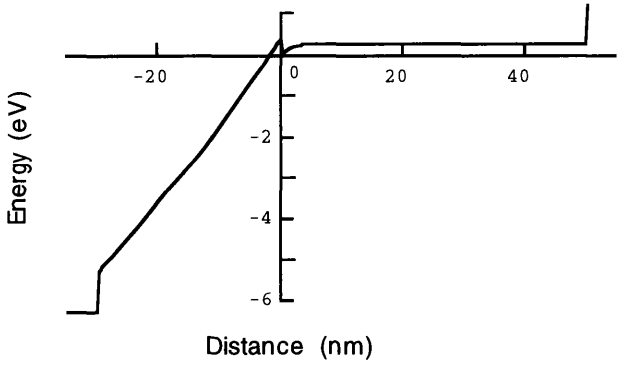

Figure 8: Band diagrams of the GaN heterostructures for doped GaN layer. Notice the difference in the electric field slopes in GaN and AlGaN related to piezoeffect (opposite polarity compared to Fig. 6). Except for the sign of the piezoelectric polarization, all parameters used in the calculation are the same as for Fig. 6.

The studies of the piezoresistance effect in GaN/AlN/GaN structure [26] point out the possibility of the "domain" structure of the top surface, which might include domains of opposite atoms (Ga or N). As can be seen from the comparison between Fig. 6 and 8, this should dramatically affect the gate leakage current. However, experimental data for AlGaN/GaN structures are consistent with the band diagram of the kind shown in Fig. 6. [25, 26] For example, Gaska et al. [25] observed very moderate gate leakage in AlGaN/GaN doped channel HEMTs up to positive 6 volts of the gate bias.

Figures 6,7, and 8 show that the piezoeffect dramatically changes the band structure both for negative and positive biases, even for a moderately doped $Al_xGa_{1-x}N$. The resulting sheet electron concentrations in the two dimensional (2D) electron gas are on the order of 10^{13} cm^{-3}. However, at these typical Al molar fractions, the doping in the AlGaN and GaN layers is equally important and still plays a dominant role in determining the sheet electron concentration in the 2D electron gas in relaxed or partially relaxed structures.

5. MAXIMUM CURRENTS AND BREAKDOWN VOLTAGES OF GaN-BASED HEMTs.

The discussion in Sections 2 and 3 shows that the effective velocity of the order $v \approx$ of $3x10^5$ m/s and the sheet carrier concentration on the order of $n_s \approx 5x10^{13}$ cm^{-2} can, in principle, be reached in GaN/AlGaN heterostructures. This corresponds to the maximum drain current of

$$I_{ds} = qn_s v_s \approx 24 \text{ A/mm}. \quad (8)$$

An estimated breakdown electric field in wurtzite GaN is on the order of 3 MV/cm [30, 31] Assuming a 5 micron long high field region (which can be realized using an offset gate design [32]), we estimate the drain breakdown voltage to be 1,500 V for the total power dissipation of 36 kW/mm! In line with these very optimistic estimates, we show in Fig. 9 the calculated output characteristics and device transconductance of an AlGaN/GaN HFET with the parameters given in Table 2. These curves were calculated using the HEMT AIM-Spice model described by Fjeldly et al. [33]

Even higher values of the current may be obtained using a multi-channel HEMT design. [5]

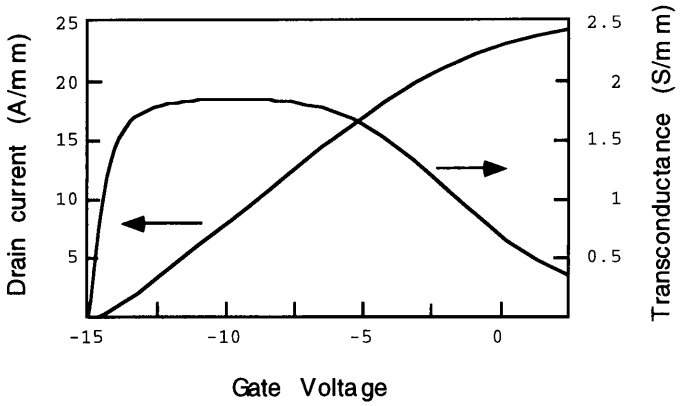

Figure 9: Calculated output characteristics and device transconductance of an AlGaN/GaN HFET in the saturation regime.

Table 2. GaN/AlGaN parameters used in Fig. 9.

AlGaN permittivity, F/m	7.97×10^{-11}
saturation velocity, m/s	3×10^{5}
threshold voltage, V	-15;
gate length, m	0.5×10^{-6}
barrier layer thickness, nm	10
2D gas effective thickness, nm	4
subthreshold ideality factor	1.5
saturation current slope, 1/V	0.01
maximum electron density, m^{-2}	$5.\ 10^{17}$
series source resistance, ohm mm	0
series drain resistance, ohm mm	0
temperature, K	300
mobility, $cm^2/V\text{-}s$	2,000
Aim-Spice delta parameter *	5
maximum 2D gas density exponent parameter *	6.
knee parameter *	2

* The meaning of these parameters of the AIM-Spice HEMT model is explained in reference [33].

The highest measured currents are typically on the order of 1 A/mm to 1.5 A/mm (see, for example{4], or Chen et al. (1997)).

The measured breakdown fields are also lower. Fig. 10 (after [32]) shows the breakdown voltage of GaN/AlGaN HEMTs as a function of the gate-to-drain distance. The breakdown field deduced from these data is on the order of 1.3 MV/cm. However, it is limited by nonuniform field distribution and will certainly be improved when the device design is optimized.

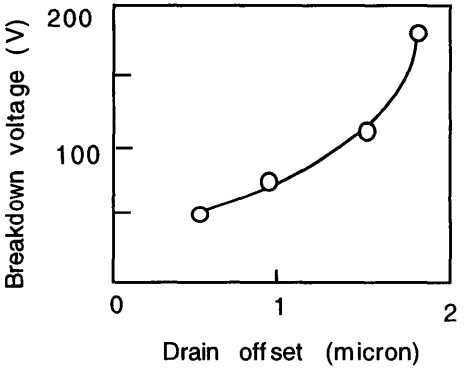

Figure 10: Breakdown voltage of GaN/AlGaN HEMTs as a function of the gate-to-drain distance (after [32]).

6. SELF-HEATING AND GaN/AlGaN HEMTs ON SiC SUBSTRATES

As follows from the estimates and measurements of the maximum currents and voltages for GaN/AlGaN HEMTs, these devices might dissipate a very large power. Therefore, problems related to self-heating become very severe, especially for devices grown on sapphire substrates, which have a low thermal conductivity. Conventional heat-sinking designs, such as a flip-chip (see, for example, [35]) can be used in order to reduce self-heating. Recent studies of GaN/AlGaN on SiC substrates showed that these substrates reduce the device thermal impedance by more than an order of magnitude (down to approximately 2 °C mm/W, i.e. about 20 times smaller than for typical GaAs power FETs. [36, 37] This allowed us to dissipate record values of the DC power (up to 0.8 MW/cm^2).

The epitaxial GaN structure grown on SiC has an advantage of a much smaller lattice mismatch (only 3-4%). Our comparative studies of the Hall mobility, Quantum Hall Effect, and Shubnikov-de-Haas effect on AlGaN/GaN heterostructures grown by MOCVD on sapphire and 6H-SiC substrates using an isolating AlN buffer show that the material quality is much better for the heterostructures grown on 6H-SiC. [7]

Both p-type and n-type SiC substrates have been used. [7] However, semi-insulating SiC substrates are expected to yield a much better microwave performance because of sharply reduced parasitics.

GaN/AlGaN HEMTS on SiC substrates exhibited a strong backgating effect. The application of bias to the SiC substrate also changes the shape of the transconductance dependence on the top gate bias. When the top gate is floating, the SiC substrate acts as the gate with the effective device transconductance on the order of 50 mS/mm, even in the devices with the distance between the substrate and the channel on the order of 0.5 micron. [7] Thinner epitaxial structures should exhibit even stronger effects related to SiC substrates and a much larger current enhancement.

7. CONCLUSIONS

Excellent transport properties of GaN-based materials and heterostructures should allow us to reach record values of currents and voltages in AlGaN/GaN HEMTs. Recent impressive experimental results are still far below of the ultimate device performance as demonstrated by the calculations reported in this paper. The device physics of AlGaN/GaN HEMTs is quite different from that of more conventional GaAs-based HEMTs because of a different role played by ionized impurity scattering and very strong piezoelectric properties. Innovative designs, such as doped channel HEMTs, HEMTs with offset gates, HEMTS grown on SiC substrates, multi-channel HEMTs and other should allow us to take better advantage of materials properties of GaN, which make this material to be superior for high-power applications.

8. ACKNOWLEDGMENT

I would like to thank my colleagues and co-authors, Drs. U. V. Bhapkar, A. D. Bykhovski, B. L. Gelmont, V. V. Kaminski, Q. Chen, S. K. O'Leary, Professor M. A. Khan, Mr. B. E. Foutz, Professor L. F. Eastman, Drs. R. Gaska, J. W. Yang, S. M. Soloviov, A. Osinsky, Professor T. Fjeldly, Drs. T. Ytterdal, C. J. Sun, W. Knap, S. Contreras, H. Alause, C. Skiberbiszewski, Professors J. Camassel, M. Dyakonov, J. L. Robert, Drs. M. Sadowski, S. Huant, F. J. Yang, M. Goiran, J. Leotin, Mr. A. Ping, Professor I. Adesida, Drs. J. Burm, W. J.Schaff, and Professor Xu who contributed to the research described in this paper. I am also grateful to Drs. R. Gaska, A. D. Bykhovski, S. K. O'Leary, and Mr. B. E. Foutz for valuable comments. This work has been supported by the Office of Naval Research and by the Cornell University under the MURI program subcontract No. N00014-97-1-1223.

9. REFERENCES

1. M. Bhatnagar and B. J. Baliga, IEEE Trans. Electron Devices, vol. 40, p. 645 (1993)
2. M. Shur and A. Khan, GaN Based Field Effect Transistors, in "High Temperature Electronics", ed. M. Willander and H. L. Hartnagel, Chapman and Hall, pp. 297-321, London (1996)
3. S. C. Binari, J. M. Redwing, G. Kelner, and W. Kruppa, Electronics Letters, 33, No. 3, pp. 242-243 (1997)
4. R. Gaska, Q. Chen, J. Yang, A. Osinsky, M. Asif Khan, and Michael S. Shur, IEEE Electron Device Letters, vol. 18, No. 10, pp. 492-494, October (1997)
5. R. Gaska, M. S. Shur, J. Yang, and T. A. Fjeldly, Double Channel AlGaN/GaN Heterostructure Field Effect Transistors, MRS, Symposium D, Spring, accepted (1998)
6. M. Asif Khan, Q. Chen, and C. J. Sun, M. S. Shur, and B. L. Gelmont, Appl. Phys. Lett., vol. 67, No. 10, Sep. 4, pp. 1429-1431 (1995)
7. R. Gaska, M. S. Shur, J. W. Yang, A. Osinsky, A. O. Orlov, G. L. Snider, Substrate Bias Effects in AlGaN/GaN Doped Channel Heterostructure Field Effect Transistors Grown on Doped SiC Substrates, to be published in Proceedings of the International Conference on SiC and Related Compounds (1997)
8. D. L. Rode and D. K. Gaskill, Appl. Phys. Lett., 66, 1972 (1995)
9. J. G. Kim, A. C. Frenkel, H. Liu, and R. M. Park, Appl. Phys. Lett., 65, 91 (1994)
10. M. S. Shur, B. Gelmont, and M. Asif Khan, J. Electronic Materials, vol. 25, No. 5, pp. 777-785 May (1996)
11. U. V. Bhapkar and M. S. Shur, J. Appl. Phys., 82 (4), pp. 1649-1655, August 15 (1997)
12. J. Xu and M. S. Shur, IEEE Trans. Electron Devices, vol. ED-34, No. 8, pp. 1831-1832, Aug. (1987)
13. B. E. Foutz, L. F. Eastman, U. V. Bhapkar, M. S. Shur, Appl. Phys. Lett., 70, No 21, pp. 2849-2851 (1997)
14. B. E. Foutz, L. F. Eastman, S. K. O'Leary, M. S. Shur, and U. V. Bhapkar, Velocity overshoot and ballistic transport in indium nitride, in Symposium Proceedings of Material Research Society, this volume (1998)

15. S. K. O'Leary, M. S. Shur, B. E. Foutz, L. F. Eastman, and U. V. Bhapkar, Velocity field characteristics of indium nitride, in Symposium Proceedings of Material Research Society, this volume (1998)
16. W. Knap, S. Contreras, H. Alause, C. Skiberbiszewski, J. Camassel, M. Dyakonov, J. L. Robert, J. Yang, Q. Chen, M. Asif Khan, M. Sadowski, S. Huant, F. J. Yang, M. Goiran, J. Leotin, and M. Shur, Appl. Phys. Lett., 70 (16), pp. 2123-2125, April (1997)
17. F. Stern, and S. Sarma, Phys. Rev., B-30, No. 2, pp. 840–848 (1984)
18. A. D. Bykhovski, B. Gelmont, and M. S. Shur, J. Appl. Phys. Dec., vol. 74 (11), p. 6734 (1993)
19. A. D. Bykhovski, B. Gelmont, and M. S. Shur, Appl. Phys. Lett., vol. 63, p. 2243 (1993)
20. A. D. Bykhovski, B. Gelmont, and M. S. Shur, J. Appl. Phys., 78 (6), pp. 3691-3696, 15 September (1995)
21. A. D. Bykhovski, B. Gelmont, M. S. Shur, and A. Khan, J. Appl. Phys., vol. 77(4), pp. 1616-1620 (1995)
22. A. D. Bykhovski, V. V. Kaminskii, M. S. Shur, Q. C. Chen, and M. Asif Khan, Appl. Phys. Lett., 68 (6), pp. 818-819 (1996)
23. A. D. Bykhovski, V. V. Kaminski, M. S. Shur, Q. C. Chen, M. A. Khan, Applied Physics Letters, November 18, 69(21), p. 3254 (1996)
24. E. T. Yu, G. J. Sullivan, P. M. Asbeck, C. D. Wang, D. Qiao, and S. S. Lau, Appl. Phys. Lett., vol. 71, No 19, pp. 2794-2796 (1997)
25. R. Gaska, J. Yang, A. Osinsky, A. D. Bykhovski, and Michael S. Shur, Piezoeffect and Gate Current in AlGaN/GaN High Electron Mobility Transistors, Appl. Phys. Lett., vol. 71, Dec. 22, (1997)
26. R. Gaska, J. Yang, A. D. Bykhovski, Michael S. Shur, V. V. Kaminski, and S. M. Soloviov, Piezoresistive Effect in GaN-AlN-GaN Structures, Appl. Phys. Lett., vol. 71, Dec. 29 (1997)
27. R. Gaska, J. Yang, A. D. Bykhovski, Michael S. Shur, V. V. Kaminski, and S. M. Soloviov, The Influence of the Deformation on the Two-Dimensional Electron Gas Density in GaN-AlGaN Heterostructures, Appl. Phys. Lett., vol. 72, Jan. (1998)
28. Martin, G., A. Botchkarev, A. Rockett, and H. Morkoç, Appl. Phys. Lett., v. 68, (18) pp. 2541-2543 (1996)
29. A. D. Bykhovski, B. L. Gelmont, and M. S. Shur, J. Appl. Phys., Vol. 81, No. 9, pp. 6332, May (1997)
30. Jan Kolnik, Ismail H. Oguzman, Kevin F. Brennan, Rongping Wang and P. Paul Ruden, J. Appl. Phys. 81 (2), pp. 726-733 (1997)
31. Ismail H. Oguzman, E. Bellotti, Kevin F. Brennan, Jan Kolnik, Rongping Wang and P. Paul Ruden, J. Appl. Phys. 81 (12), pp. 7827-7824 (1997)
32. R. Gaska, Q. Chen, J. Yang, A. Osinsky, M. Asif Khan, and Michael S. Shur, Electronics Letters, 33, No. 14, pp. 1255-1257, 3 July (1997)
33. T. Fjeldly, T. Ytterdal, and M. S. Shur, Introduction to Device and Circuit Modeling for VLSI, John Wiley and Sons, 1997
34. Q. Chen, R. Gaska, M. Asif Khan, Michael S. Shur, A. Ping, I. Adesida, J. Burm, W. J.Schaff, and L. F. Eastman, Electronics Letters, vol. 33, No. 7, pp. 637-639, March 27 (1997)
35. M. S. Shur, GaAs Devices and Circuits, Plenum, New York (1987)
36. R. Gaska, A. Osinsky, J. Yang, and Michael S. Shur, Self-Heating in High Power AlGaN/GaN HFETs, IEEE Electron Device Letters, vol. 19, No. 2, February (1998)
37. R. Gaska, J. Yang, A. Osinsky, M. Asif Khan, M. S. Shur, Novel High Power AlGaN/GaN HFETs on SiC substrates, IEDM-97 Technical Digest, December (1997)